analytical chemistry

Article

pubs.acs.org/ac

A Generalizable, Tunable Microfluidic Platform for Delivering Fast Temporally Varying Chemical Signals to Probe Single-Cell Response Dynamics

Loice Chingozha,[†] Mei Zhan,[§] Cheng Zhu,[§,¶,‡] and Hang Lu*[,†,§]

[†]School of Chemical & Biomolecular Engineering, Georgia Institute of Technology, Atlanta, Georgia 30332, United States

[§]Interdisciplinary Program in Bioengineering, Georgia Institute of Technology, Atlanta, Georgia 30332, United States

[‡]Wallace H. Coulter Department of Biomedical Engineering, Georgia Institute of Technology and Emory University, Atlanta, Georgia 30322, United States

[¶]School of Mechanical Engineering, Georgia Institute of Technology, Atlanta, Georgia 30332, United States

Supporting Information

ABSTRACT: Understanding how biological systems transduce dynamic, soluble chemical cues into physiological processes requires robust experimental tools for generating diverse temporal chemical patterns. The advent of microfluidics has seen the development of platforms for rapid fluid exchange allowing ease of changes in the cellular microenvironment and precise cell handling. Rapid exchange is important for exposing systems to temporally varying signals. However, direct coupling of macroscale fluid flow with microstructures is potentially problematic due to the high shear stresses that inevitably add confounding mechanical perturbation effects to the biological system of interest. Here, we have devised a method of translating fast and precise macroscale flows to microscale flows using a monolithically integrated perforated membrane. We integrated a high-density cell trap array for nonadherent cells that are challenging to handle under flow conditions with a soluble chemical signal generator module. The platform enables fast and repeatable switching of stimulus and buffer at low shear stresses for quantitative live, single-cell fluorescent studies. This modular design allows facile integration of any cell-handling chip design with any chemical delivery module. We demonstrate the utility of this device by characterizing heterogeneity of oscillatory response for cells exposed to alternating Ca^{2+} waveforms at various periodicities. This platform enables the analysis of cell responses to chemical perturbations at a single-cell resolution that is necessary in understanding signal transduction pathways.

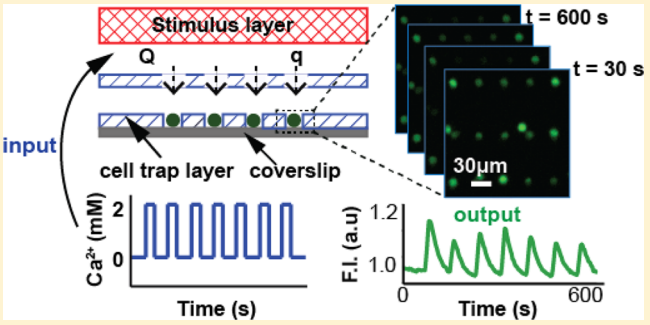

Cellular environments are inherently dynamic and generally involve complex, temporally varying signals; therefore, there is large interest in studying how dynamic extracellular signals are transduced into intracellular signals and give rise to emergent properties.[1,2] The influence of temporal dynamic inputs in biological systems has been demonstrated through observing cellular response to chemical perturbations in the form of constant stimulation, step inputs, and waveforms.[3−5] Robust tools that can provide a variety of well-tuned chemical input signals to biological systems are fundamental to deducing signal transduction pathways. Importantly, the temporal dynamics of biological system signals span a large dynamic range (seconds to days) with variable patterns that necessitates the need to develop devices that can reliably generate complex chemical signals precisely and repeatedly. These tools together with the ability to perform real-time fluorescent imaging enable simultaneous system perturbation while observing system response.

Microfluidic systems have emerged as tools for ease of fluid handling due to the predictable laminar flow and incorporation of other microfluidic components such as valves and off-chip components that facilitate precise microenvironment control.[6] Several microfluidic devices have been developed for the application of spatiotemporal chemical gradients using interface shifting in laminar coflow,[4] on- and off-chip valves, flow switching,[7] diffusion through porous membranes,[8,9] and acoustic waves.[10] These platforms that enable precise modulation of dynamic chemical environment have been developed for small organisms like the nematode,[5,11] for unicellular organisms such as bacteria[12] and yeast,[1] and for mammalian adherent cells.[2,8,13] However, many of these systems lack the ability to accommodate nonadherent cells because nonadherent cells need to be secured in place to

Received: May 23, 2014
Accepted: September 25, 2014
Published: September 25, 2014

   dx.doi.org/10.1021/ac5019843 | *Anal. Chem.* 2014, 86, 10138−10147

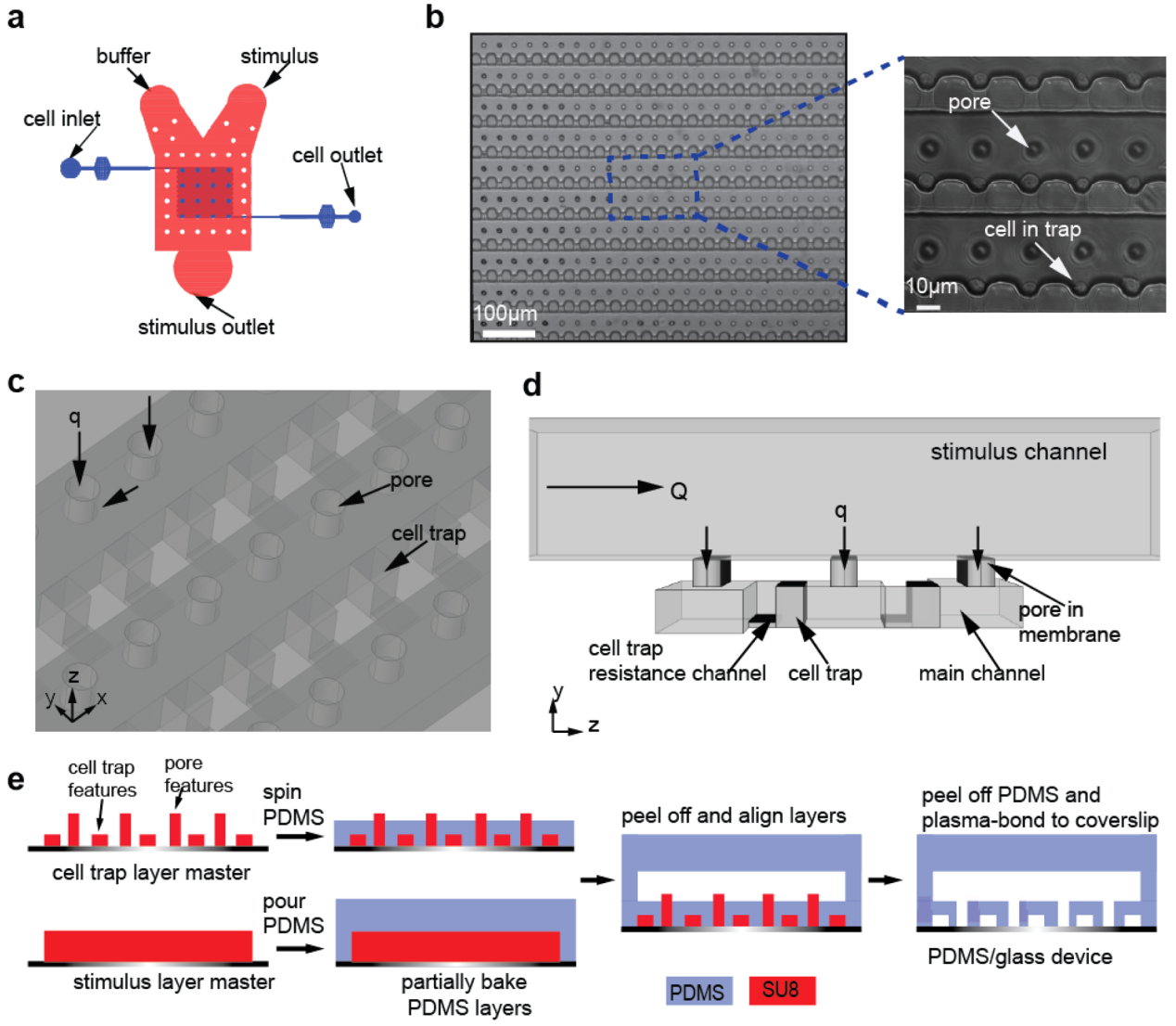

Figure 1. Multilayer design enables fast exchange of fluids for dynamic cell stimulation. (a) Top view depiction of the device showing the cell trap module (blue) and the stimulus delivery module (red), (b) top view micrograph of the cell trapping module with an array of 10 μm cell traps and 10 μm pores (the device array consists of 1000 cell traps on a 1 mm^2 footprint, and a micrograph showing cells trapped in device), (c) 3D rendering of the fluid channels showing the cell trap channels and the perforated holes in the membrane, and (d) cross-sectional depiction of the cell trapping and stimuli delivery modules. Soluble cues are introduced through the second layer using off-chip pinch valves and into the first layer through the pores. (e) Fabrication process of the device master molds and the 2-layer PDMS devices using soft lithography techniques.

prevent drifting during real-time live imaging while applying the soluble stimulus. Coupling of cell-trapping devices that secure nonadherent cells in place with a chemical signal generator would enable high-throughout, single-cell analysis with single cell resolution to an external stimulus. Therefore, a much more generalizable approach would be useful in integrating these different chip designs with signal generators. A plethora of platforms has been developed for handling suspension cells, allowing precise spatial positioning of individual cells for single-cell analysis using dielectrophoresis (DEP), hydrodynamic flow and geometric restrictions,[14,15] microwells,[16] optical tweezers,[17] and acoustic waves.[18]

Here, we have developed a technique to couple arbitrary chip design with a chemical signal generator using a perforated PDMS membrane. The design utilizes precisely controlled small convective transfer for fast fluid exchanges; this guarantees low shear stresses on the cells, while ensuring rapid switching of chemicals in a repeatable manner. We combined a high-density cell trap[15] for handling a large array of nonadherent cells with a module for the delivery of precisely tuned dynamic chemical signals to individual cells. The high-density cell trap physically confines individual cells in defined positions in a deterministic manner for robust, time-lapse imaging without cell displacement. To demonstrate the utility of our design, we show how oscillating extracellular Ca^{2+} at various periods can modulate the intracellular Ca^{2+} dynamics in Jurkat T cells.

EXPERIMENTAL METHODS AND MATERIALS

Device Fabrication. The two-layer devices were fabricated in PDMS (Dow Corning Sylgard 184, Essex-Brownwell Inc.), and negative master molds were fabricated in SU8 (Microchem) using the standard multilayer soft lithography techniques[19] as shown in Figure 1. The master mold for the cell trap module was fabricated in a three-step photolithography process with heights of 2, 15, and 15 μm, respectively,

dx.doi.org/10.1021/ac5019843 | Anal. Chem. 2014, 86, 10138−10147

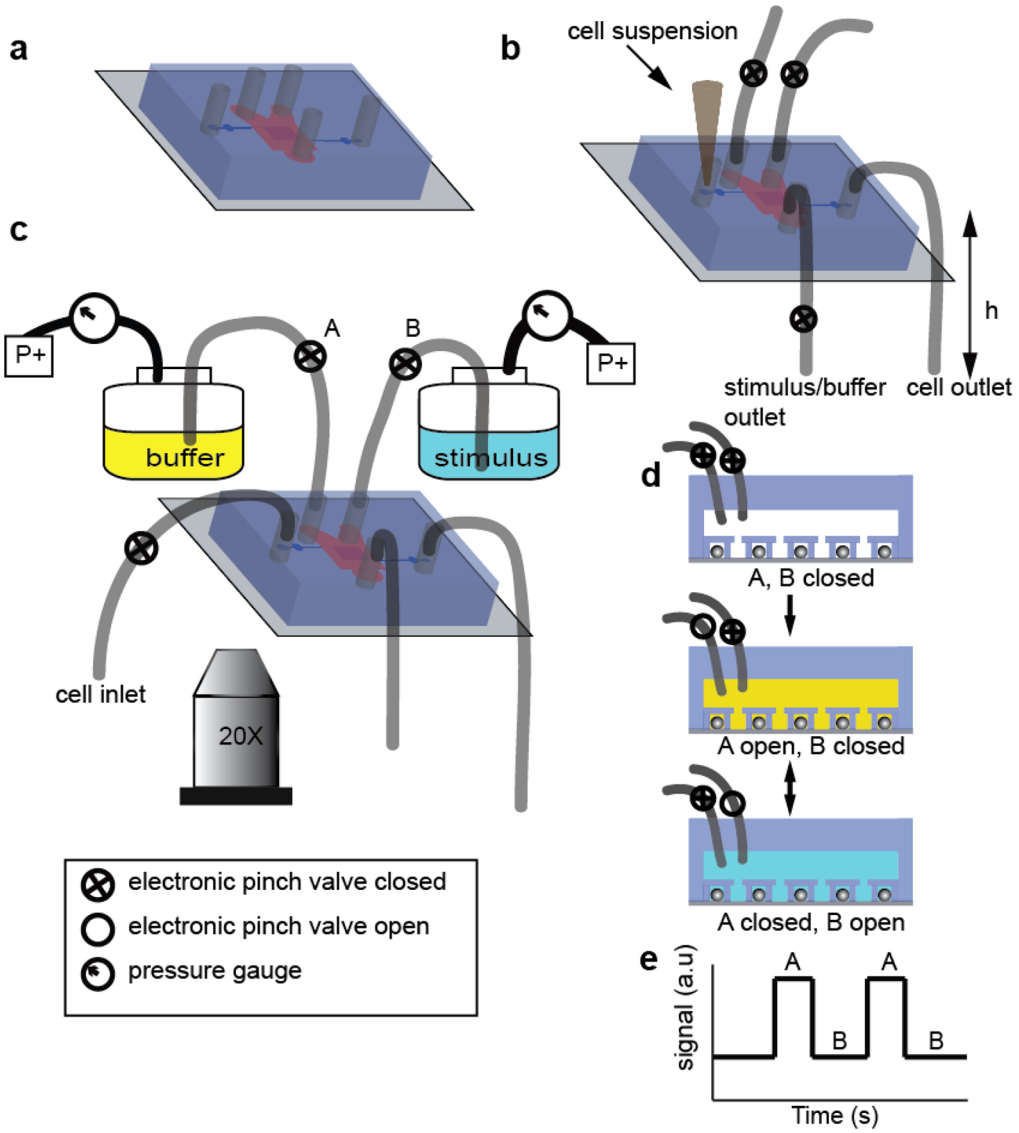

Figure 2. Schematics for device setup. (a) Depiction of the device with access holes punched, showing the cell trap layer (blue), and the stimulus layer (red), (b) cell loading (a pipet tip containing the cell suspension was placed in the cell inlet, and cells were loaded by gravity-driven flow, while the top chamber inlets and outlets were closed with pinch valves), (c) schematic of the device connections (the stimulus and buffer inlets were connected to pressure reservoirs maintained at a pressure of 1 psi, and flow into the device is controlled by the opening and closing of the electronic pinch valves), (d) depiction of the flow control during cell stimulation (valve A and valve B are in an open or closed confirmation at any given time to allow the flow of stimulus or buffer for a user-defined period of time in an automated manner using custom-made software), and (e) illustration of the oscillatory signals generated in the device.

fabricated with SU8 2002, SU8 2005, and SU8 2010. The first two layers make the cell-trapping module, and the third layer is an array of micro posts for making the pores in PDMS. The mold for the stimulus chamber was 50 μm, fabricated with SU8 2050. The negative molds were exposed to silane vapor, tridecafluoro-1,1,2,2-tetrahydrooctyl-1-trichlorosilane (UCT Special Ties, LLC) in a desiccator to allow release of the PDMS mold from the SU8 mold. For the PDMS devices, 10:1 PDMS prepolymer to cross-linking ratio was spun on the cell trap master mold to make a thin layer (~10−12 μm) encompassing the cell-trapping module with the PDMS mold being thinner than the micro posts such that the posts were still protruding to make pores in the PDMS layer. The mold was partially cured at 70 °C for 15 min, aligned, and then thermally bonded to a partially cured PDMS mold of the stimulus chamber, also made from 10:1 PDMS prepolymer to cross-linker ratio. The assembled mold was baked for complete curing of the PDMS overnight. Access holes were punched at the inlets and outlets with a 19-gauge blunt needle, and the two-layer device assembly was plasma-bonded to a coverslip.

Cell Preparation. Jurkat E6-1 human acute T lymphoma cells (ATCC) were cultured in RPMI 1640 medium with 2 mM L-glutamine and HEPES (ATCC) supplemented with 10% fetal bovine serum (Sigma-Aldrich) and 100 units mL^{-1} penicillin−streptomycin (Life Technologies), in a 37 °C, 5% CO_2 humidified incubator. For the cytosolic Ca^{2+} level measurements, cells were loaded with 5 μM Fluo3-AM (Life Technologies) calcium indicator dye in Hank's balanced salt solution (HBSS) without calcium and 0.02% pluronic acid (Sigma-Aldrich) to enhance calcium dye uptake by cells for 30 min at room temperature and washed with HBSS without calcium (Cellgro). Cells were then pretreated with 1 μM

dx.doi.org/10.1021/ac5019843 | Anal. Chem. 2014, 86, 10138−10147

thapsgargin (Sigma-Aldrich) in HBSS without calcium for 5 min before being loaded in the device by gravity-driven flow. Thapsgargin depletes the intracellular calcium stores,[20] which facilitates the opening of the calcium-activated release channels (CRAC) allowing entrance or exit of Ca^{2+} from the cytosol into the extracellular space. Cells were exposed to oscillatory Ca^{2+} signals of varying frequencies while images were acquired every 2 s for 30 min on a fluorescent inverted microscope.

Device Setup and Operation. The devices were primed with HBSS with 2% bovine serum albumin (Sigma-Aldrich) to prevent nonspecific cell adhesion to the device surface and remove bubbles from the device. The stimulus/buffer chamber inlets were connected to two pressurized reservoirs set at a pressure of 1 psi, one containing HBSS with 2 mM EGTA and the other HBSS with 1.5 mM Ca^{2+}. Cells were loaded into the cell trap module using gravity-driven flow (~4 kPa) corresponding to a flow rate of ~5 μL/h as shown in Figure 2a. Figure 2b shows how the device was connected to pressure reservoirs containing the buffer and stimulus. Once the cells were loaded, alternating solutions of the 1.5 mM Ca^{2+} and EGTA buffer were delivered to the cells using off-chip pinch valves at user-defined durations with simultaneous fluorescence imaging to track calcium dynamics, as indicated by the reporter Fluo-3 AM, in individual cells. Valve control and image acquisition were performed using custom MATLAB-based scripts (Mathworks Inc.).

Signal Delivery Characterization. The flow profiles and mass transport in the device were characterized using a lumped resistance analysis model (3-dimensional COMSOL Multiphysics model) and empirically using a fluorescent dye. The delivery of chemical cues into the cell trap chamber was characterized using fluorescein dye with cells loaded in the device. Briefly, alternating solutions of fluorescein (50 μg/mL) in PBS and PBS in pressurized reservoirs were delivered to the stimulus chamber at user-defined oscillating periods (2 s–2 min) using off-chip electronic pinch valves, while simultaneously acquiring fluorescence images at 10 fps. Fluorescence intensity of the images was measured at all the rows in the cell trap chamber to determine the delivery of signal from the stimulus chamber to the cell trap channel.

Imaging and Data Analysis. Images were acquired every 2 s for 30 min on a fluorescent microscope using MATLAB interfaced with Micromanager Software[21] for image acquisition and automated valve control. All of the image processing and analysis was performed with custom-made scripts in MATLAB. Briefly, to analyze the calcium dynamics, the average intensity for each cell was determined and in every frame, the background was subtracted from the mean intensity for the individual cell being analyzed. The mean intensity for each cell was then normalized to the initial intensity to account for the differences in the initial dye loading for each cell. The average response for the cell population was also computed at each time point.

RESULTS AND DISCUSSION

Design of a Modularized Device for Cell Stimulation. The measurement of cell response to temporally varying soluble chemical cues can provide insights on the signal transduction pathways. Here, we are interested in evaluating cell response to dynamic stimulation at single-cell resolution. Therefore, we need cell trap arrays to handle a large number of cells while simultaneously applying dynamic chemical cues in a robust manner. To address this challenge, we developed a two-layer PDMS device consisting of two modules: a cell-trapping module and stimulus module capable of generating temporal signals as depicted in Figure 1a. For the cell trap layer shown in Figure 1b, we interface microstructures for single-cell immobilization and micropores on a thin PDMS membrane. The cell trap module consists of an array of 10 μm cell traps on a thin membrane perforated with holes of 8–10 μm in diameter, with each device having 1000 cell traps (Figures 1b and S1, Supporting Information). The micropores on the membrane provide a fluid connection between the cell trap layer and the top stimulus delivery chamber (Figure 1b,c) that facilitate faster switching of stimulus and buffer. This enables the ability to study cellular response to a wide range of temporal patterns, by avoiding dead volume effects of the chip peripherals such as tubing and dead space upstream of the experimental area.

In our design, we sought to minimize shear stress experienced by cells in the device during delivery of chemical stimulation. Flow-based stimulus delivery can inevitably exert shear stresses on cells, which have been demonstrated to be capable of altering cell physiology.[22,23] It is therefore important to ensure that the device is operated at low shear stress to have a controlled effect on cell response. The shear stress experienced by the cells is proportional to the flow rate q that goes through the cell trap module (Figures 1c,d and S2, Supporting Information).

The goal is to balance the needs to minimize q, to have low (<10 dyn/cm^2) shear stresses, and to rapidly deliver a precise soluble chemical stimulus. The design principle we use here is based on the relative resistances of the stimulus chamber ($R_{\text{stimulus chamber}}$) and the cell trap chamber ($R_{\text{cell trap}}$) to which the soluble cues will be delivered. These relative resistances determine how the input flow rate Q decomposes into the cell trap flow rate, q, and the stimulus chamber flow rate, $Q - q$ (Figure S2, Supporting Information). The lateral dimensions of the stimulus chamber were determined by the overall size of the cell trap chamber. In our case, the stimulus chamber had a lateral dimension of 2 mm by 2 mm and a height of 50 μm. The relative resistances were modulated by changing the dimensions of the cell trap membrane chamber. Figure S2, Supporting Information, shows the flow-resistance components the system, where the resistance of the system is contributed by $R_{\text{stimulus chamber}}$ (low resistance), $R_{\text{cell trap}}$ (high resistance), and the resistance R_{pore} of the pores in the membrane (high resistance). The resistance of the bottom chamber is a combination of R_{pore} and $R_{\text{cell trap}}$. The membrane resistance depends on the underlying chip design of the cell trap and the dimensions of the pore diameter (D_{pore}), length (L_{pore}), and number of pores (N_{pore}). The pore dimensions are user-defined during mask design (D_{pore}, N_{pore}) and in the fabrication steps (L_{pore}) and are subject to printing and lithography resolution and aspect ratio restrictions. In our studies, we experimentally varied the pore dimensions (D_{pore} from ~10 μm, L_{pore} from ~10 μm, and N_{pore} from 800 pores) and theoretically determined the flow resistance and average velocity (2.7 mm/s) in the cell trap chamber. The pore dimensions would affect the resistance of the membrane and therefore determine the flow rates through the cell trap. With these designs, we characterized the fidelity of the signal in the device over a large temporal range. Within the range of these parameters, we did not observe differences in the performance of our device.

The optimal designs allowed us to keep the flow rate in the cell chamber relatively small and, therefore, shear stress under

dx.doi.org/10.1021/ac5019843 | Anal. Chem. 2014, 86, 10138–10147

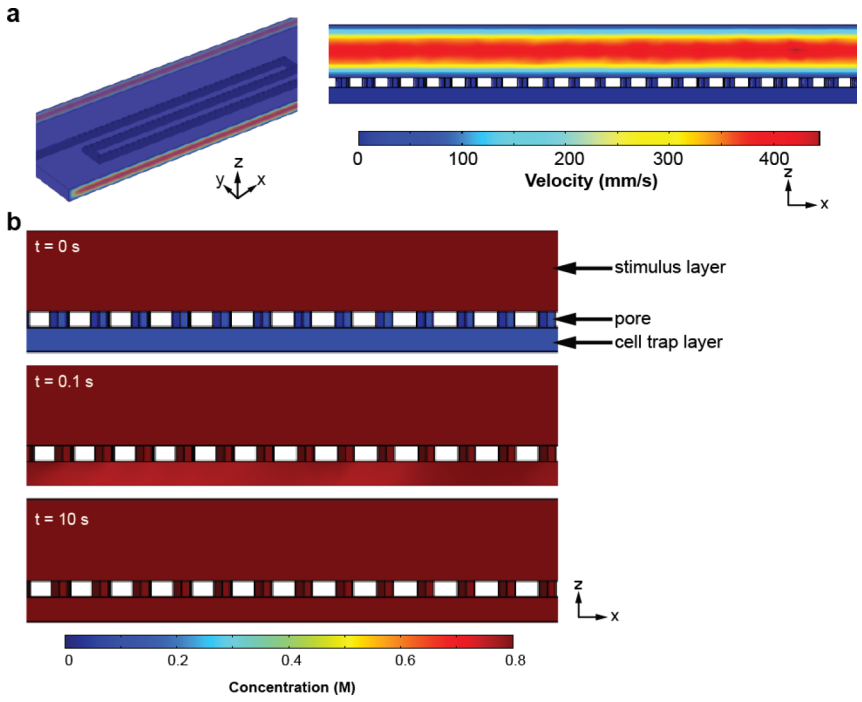

Figure 3. Fluid and mass transfer numerical simulation results. (a) Fluid flow and (b) mass transfer of a solute for a time of 0, 0.1, and 10 s after a solution containing a solute of concentration 0.8 M was introduced into the device, demonstrating that the concentration profile at 0.1 s was already very close to steady state distribution.

control yet still be able to obtain high fidelity in the signal delivery. The input flow rates into the stimulus chambers were measured to be ~0.5 mL/min resulting in an exchange time of 6 ms in the stimulus chamber, which translates to theoretical flow rates of 1−10 μL/h in the cell trap chamber. At these flow rates, the corresponding wall shear stress was 0.1−5 dyn/cm^2, estimated from the flow rate, q, in the cell trap chamber. In calculating the wall shear stress, we assume that the device traps are occupied and therefore the width of the channel is roughly the same as the width of the main channel in the cell trap chamber. The tunability of the device design will allow a user to vary the device dimensions to fit the need. However, there is a trade-off between high temporal resolution and low shear stresses. In general, in order to achieve a high temporal resolution while maintaining low shear stress, we can vary the pore dimensions or the overall size of the device. In summary, our design has achieved a low shear stress by increasing the resistance of the cell trap module by changing the parameters in Figure S2, Supporting Information, and the adequate time resolution of signals for the system of interest. We further characterized the device performance using COMSOL. Figure 3a shows the steady-state flow profile of the truncated version of the devices showing the first three rows. From the simulation, the average velocity in the cell trap chamber was 2 mm/s, similar to the average velocity determined from the lumped resistance model (2.73 mm/s). The flow profile was then used to analyze transient mass transfer from the stimulus chamber into the cell trap region for a period of 10 s. The steady concentration in the cell trap region was reached within 200 ms (Figure 3b).

Generation of Robust Dynamic Stimulus at a Wide Range of Frequencies. To characterize the synchrony and the rise-time in the temporal delivery of chemicals in the device, we pulsed the chamber with alternating solutions of PBS and fluorescein dye in PBS with cells loaded in the device at varying periodicities (2 s to 2 min). When stimulating a large population of cells with soluble chemicals, it is crucial to ensure synchrony and robust control of temporal signal delivery. We measured the average fluorescence intensity of a selected region, at different positions on the device as depicted in Figure 4a. As shown in Figure 4b,c for a signal of a repeated 20 s period, the waveforms are synchronized for all 10 rows of the cell trapping chamber assayed within the device and are of similar amplitudes. In addition, the generation of the signal is repeatable throughout the duration of the experiment (Figure 4b). This demonstrates that the cells loaded in our platform experience the same signal simultaneously. Ensuring that the cells receive the same signal is critical in studying cell-to-cell variations in a population such that the differences observed between cells can be attributed to the inherent cell population heterogeneity rather than an artifact of the experiment. The delivery of spatially independent stimulus is enabled by the stimulus chamber having a very low resistance compared to the cross membrane resistance and cell trap chamber allowing a small amount of the stimulus to bleed through from the stimulus chamber to the cell trap layer through the pores in the membrane. In Figure 4d, we show that the signal is uniform within each row by measuring the signal intensity at different positions in an individual row, showing that the asymmetric positioning of the stimulus inlets do not affect the uniformity of the signal in the cell trap chamber. We further quantified the differences in the signal between the upstream and downstream traps and found a negligible difference in the periodicity (<0.01%) between the upstream and downstream rows (Figure 4e) in the device. The average rise-time was determined to be ~154 ± 0.1 ms which is consistent with our COMSOL simulations (<200 ms). Similar observations were made at a lower period of 5 s as shown in Figure S3, Supporting Information.

dx.doi.org/10.1021/ac5019843 | *Anal. Chem.* 2014, 86, 10138−10147

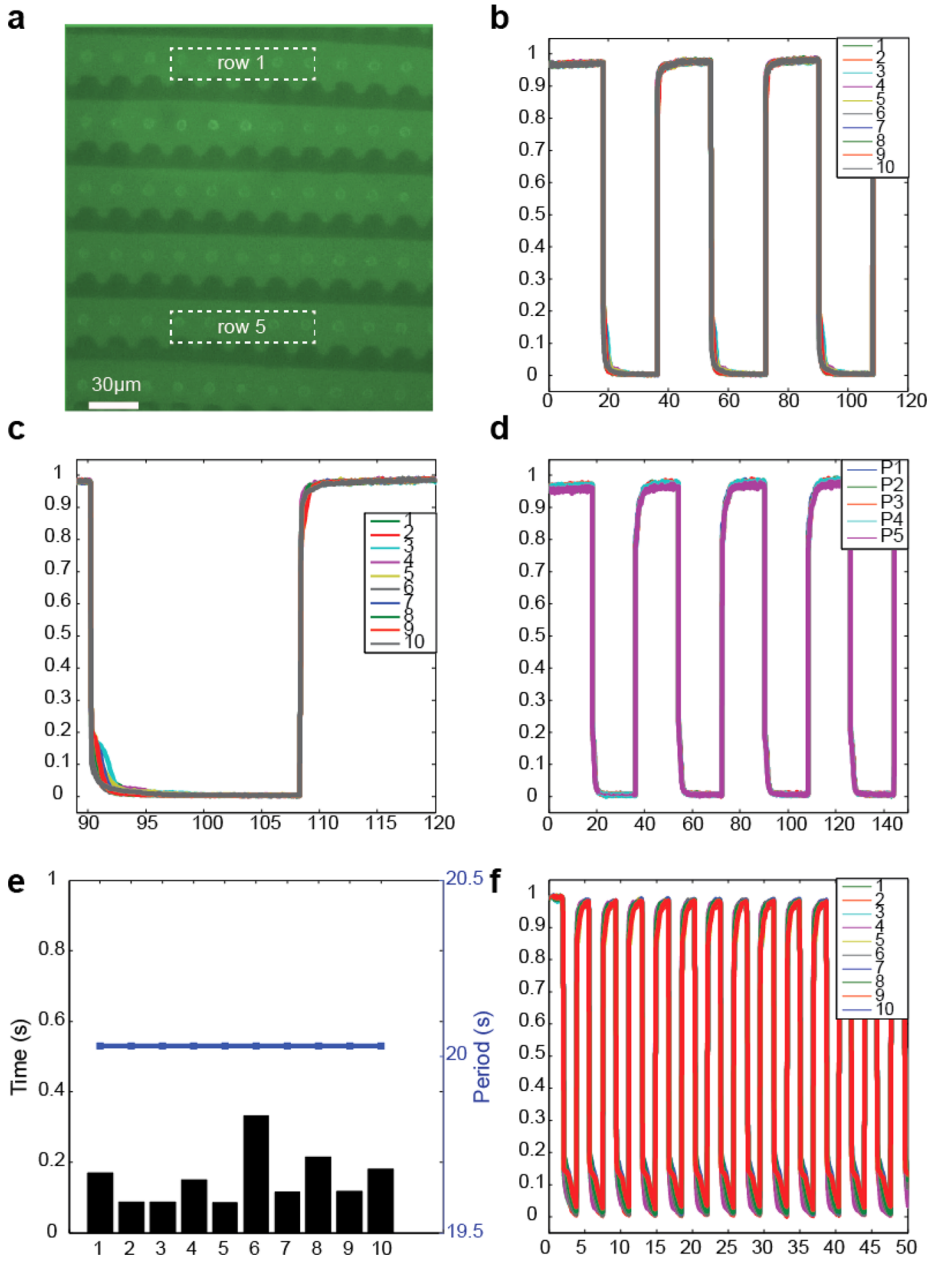

Figure 4. Spatially independent waveforms generated over a large temporal dynamic range with rapid rise and small delay. The signal delivery in the device was characterized by flowing alternating PBS solutions with and without fluorescein at different periodicities. (a) Micrograph for pulse visualization using fluorescence dye. (b) 20 s waveforms at different rows on the device demonstrating the uniformity of the pulses throughout the device. At each row, a representative area was selected (dotted region in (a)) to measure the intensity of the signal. (c) Zoomed in section of (b) to demonstrate how the signal traces at different rows in the device overlap. (d) Plot of signal traces at different positions on the devices on the same row demonstrating uniformity of the signal within each cell trap row in the device. (e) Plot of the period (right-hand *y* axis) and the rise-time (left-hand *y* axis) for the 10 rows of traps in the device, showing there are negligible differences between the top and the bottom row periodicities and rise-time. The average rise-time is ∼150 ms, and (f) the lowest period achieved (2 s) without the need to change the flow rates in the stimulus chamber and with negligible changes in the flow rates in the cell trap module.

In addition to achieving a spatially uniform signal, we evaluated the signal temporal resolution of the device that is crucial for the versatility in applications of biological systems. Biological processes span a large dynamic range, from short-time scales in calcium oscillations to hours in gene transcription, and being able to use the same tool for probing different processes would be advantageous. Overall, we achieved a temporal resolution on the order of seconds for the signal delivery without changing the flow rates in the device, thus maintaining low shear stress throughout the study. We determined from the flow rate and shear stress calculations that the lowest achievable period would be ∼4 s while keeping the shear stress below 10 dyn cm^{-2}. Figure 3f shows that the device can be used to deliver input signals with periods as short as 2 s, indicating that, for any pattern of signal, the smallest period would be 2 s. Furthermore, reducing the volume of the cell trap chamber can increase the temporal resolution while maintaining low shear stress. The ability to deliver high frequency chemical signals makes our platform versatile in applications

dx.doi.org/10.1021/ac5019843 | *Anal. Chem.* 2014, 86, 10138−10147

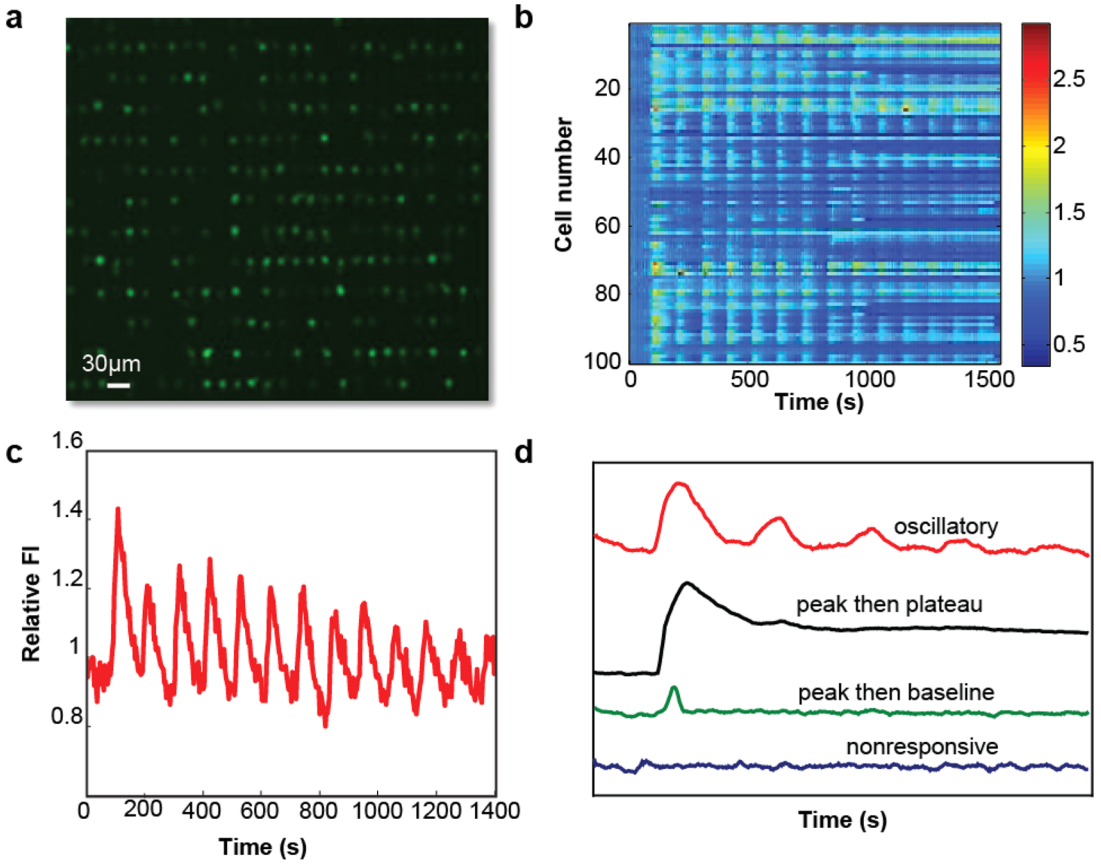

Figure 5. Analysis at single cell resolution shows heterogeneity in cell response to extracellular calcium stimulation. Jurkat cells loaded with cytoplasmic calcium indicator Fluo3-AM and treated with thapsargin were exposed to an environment with Ca^{2+} concentration oscillating between 0 and 1.5 mM at different periodicities. (a) Fluorescence micrograph of cells loaded with calcium indicator Fluo3-AM in device. (b) Heat map for individual cell response to extracellular Ca^{2+} pulses. The colors indicate low (blue) and high (red) cytoplasmic calcium concentrations. (c) The average of fluorescence intensity for the cells shown in (b) exhibit an overall oscillatory response. (d) From the analysis of the cell fluorescence intensity over time, four distinct calcium response curves were observed: (1) oscillations that were entrained with the frequency of the Ca^{2+} input signal, (2) a peak at first pulse followed by a plateau at a level higher than the baseline level, (3) a peak at the first exposure followed by a drop to the baseline level, and (4) no response to the stimulation. The results are representative of three similar experiments.

over a large temporal dynamic range important for probing biological systems of different time scales.

The fidelity in the signal delivery is achieved by the key feature in our design: monolithic integration of a perforated PDMS membrane with cell-trapping microstructures. The predefined perforations in the PDMS membrane enable stimulus and buffer delivery from the stimulus chamber bulk flow into the cell trap area using off-chip pinch valves. Using vertical flow to exchange fluids in the cell trap allows the entire cell trapping layer to be exposed to the same concentration of stimulus at the same time and circumvents diffusion that would otherwise limit the temporal resolution of the signal delivery. Moreover, having a monolithically integrated membrane makes this approach generalizable to existing microfluidic platforms for delivering soluble cues. Furthermore, using PDMS to make the perforated membrane rather than using commercial membranes not only enables the integration with cell-handling microstructures but also enables ease of fabrication of the device using established soft lithography methods for thermal bonding of PDMS to PDMS and plasma-bonding the PDMS assembly to glass. Even though our device is a multilayer PDMS device, which adds to the complexity of the fabrication, the alignment of the two layers does not require a microscope, and the cells will be in contact with the coverslip, which also allows for high-resolution imaging.

Heterogeneous Cellular Response to Oscillatory External Ca^{2+} Signal. To demonstrate the utility of the device in stimulating a large number of cells and obtaining single-cell data, we measured changes in cytosolic calcium in Jurkat cells exposed to alternating solutions of Ca^{2+} and EGTA, a calcium chelator. Calcium is a ubiquitous messenger in a number of physiological processes including immune cell response to antigen stimulation.[24,25] In addition, calcium oscillations have been observed in both excitable and nonexcitable cells, and differential immune response and gene expression have been attributed to varying calcium oscillation.[26,27] In general, the different calcium dynamics would affect cell signaling, ultimately leading to differences in cellular function. The ability to experimentally modulate these calcium oscillations with high temporal resolution would provide an experimental tool in studying the physiological function of calcium oscillations. As a demonstration of the capabilities of our device, we measured changes in cytosolic Ca^{2+} levels in Jurkat T cells loaded with Fluo3-AM Ca^{2+} dye (Figure 5a) exposed to Ca^{2+} solution waveforms. To induce Ca^{2+} oscillations in Jurkat cells, the cells were first treated with thapsgargin to deplete the intracellular calcium stores, inhibit

dx.doi.org/10.1021/ac5019843 | Anal. Chem. 2014, 86, 10138−10147

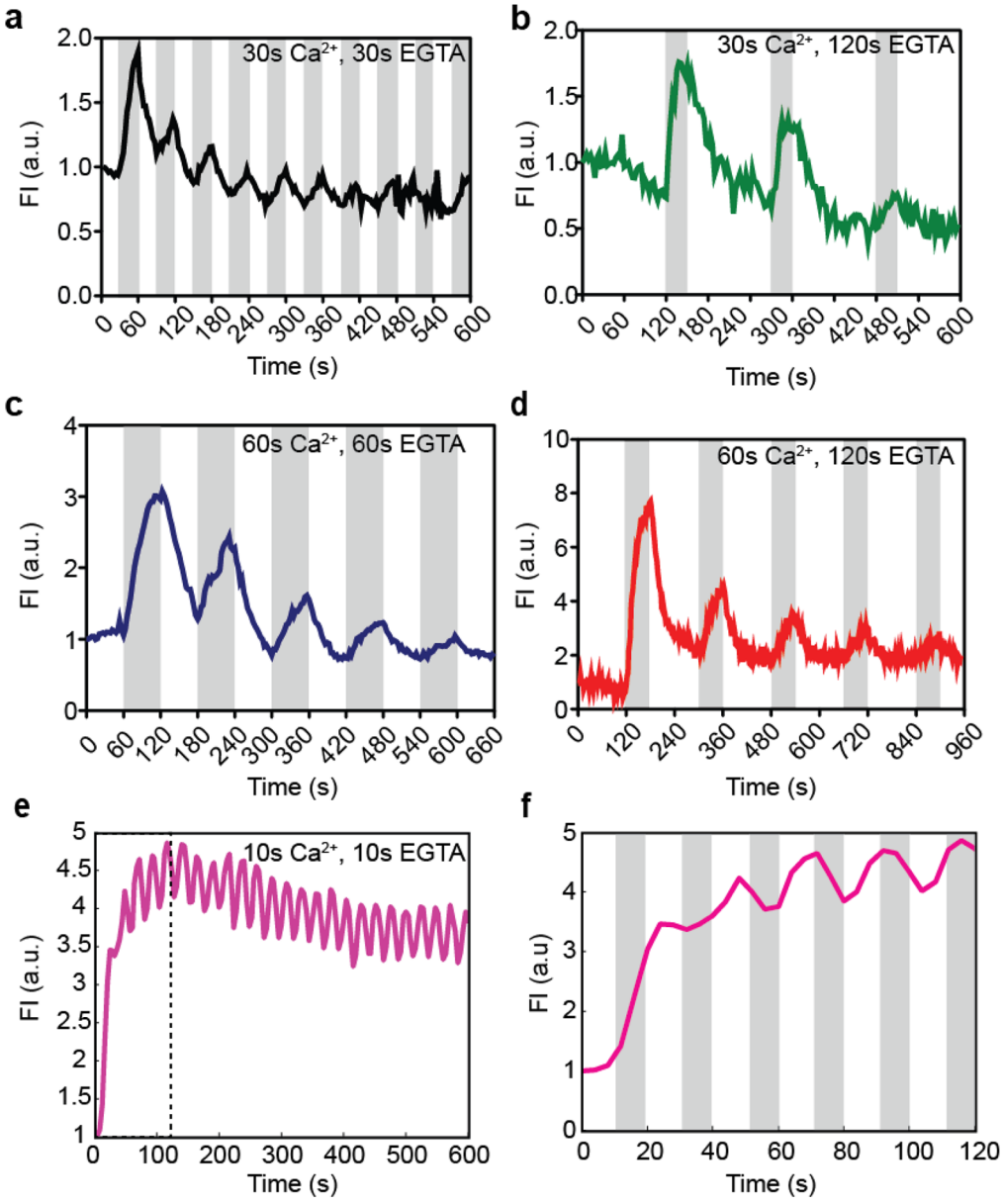

Figure 6. Responses of cells to different periodic stimuli. (a–e) Average cytoplasmic calcium dynamics to oscillating external Ca^{2+} concentration. The cells were exposed to dynamic Ca^{2+} concentration oscillating between 0 and 2 mM at different periodicities as indicated on the panels. The figure plots the average fluorescence intensity indicative of changes in cytosolic Ca^{2+} over time. The gray bars show the periods at which the Ca^{2+} buffer was applied. Cells showed an increase in fluorescence intensity within 1 s of exposure to Ca^{2+} with diminishing amplitude with subsequent stimulations. By modulating the extracellular Ca^{2+} concentration, we are able to create temporally varying cytosolic Ca^{2+} signals inside the cells. The ability to generate oscillations at different periodicities in the cells will enable the study of how the nature of oscillations have an effect on gene expression patterns and cell behavior. (f) Zoomed in image of the 10 s period stimulation showing that at this frequency the cell response signals show a lag compared to the input signal.

the calcium ATPases, and open up the CRAC channels as previously described.[26] It has been reported that the depletion of the intracellular stores (endoplasmic/sarcoplasmic reticulum) triggers external Ca^{2+} entry through the activation of the CRAC channels. The source of Ca^{2+} oscillations in immune cells has been attributed to the transport of extracellular Ca^{2+} through the CRAC channels; therefore, this experimental approach offers a relevant platform for studying signaling pathways driven by calcium oscillations.[27]

We analyzed the dynamic cytosolic Ca^{2+} response when cells were exposed to different extracellular concentrations of Ca^{2+}, achieved by alternating solutions of Ca^{2+}-rich (HBSS with 2 mM Ca^{2+}) and Ca^{2+}-poor buffer (HBSS with EGTA) at different periodicities. In Figure 5, we show representative results from at least 3 similar experiments where cells were exposed to Ca^{2+} for 20 s and EGTA for 100 s. In Figure 5b, individual calcium traces are plotted and show differences in the magnitude of the calcium levels within a population. Each row represents an individual cell, and the color represents the intensity of the dye with red being high and blue low. The differences in intensity show the inherent heterogeneity between cells that might explain functional differences observed in response to signaling processes dependent on the amplitude of a signal encoded by cytoplasmic Ca^{2+}. In addition, similar trends were observed in independent experiments (n = 3), and Figure S-2, Supporting Information, shows another example of

dx.doi.org/10.1021/ac5019843 | Anal. Chem. 2014, 86, 10138–10147

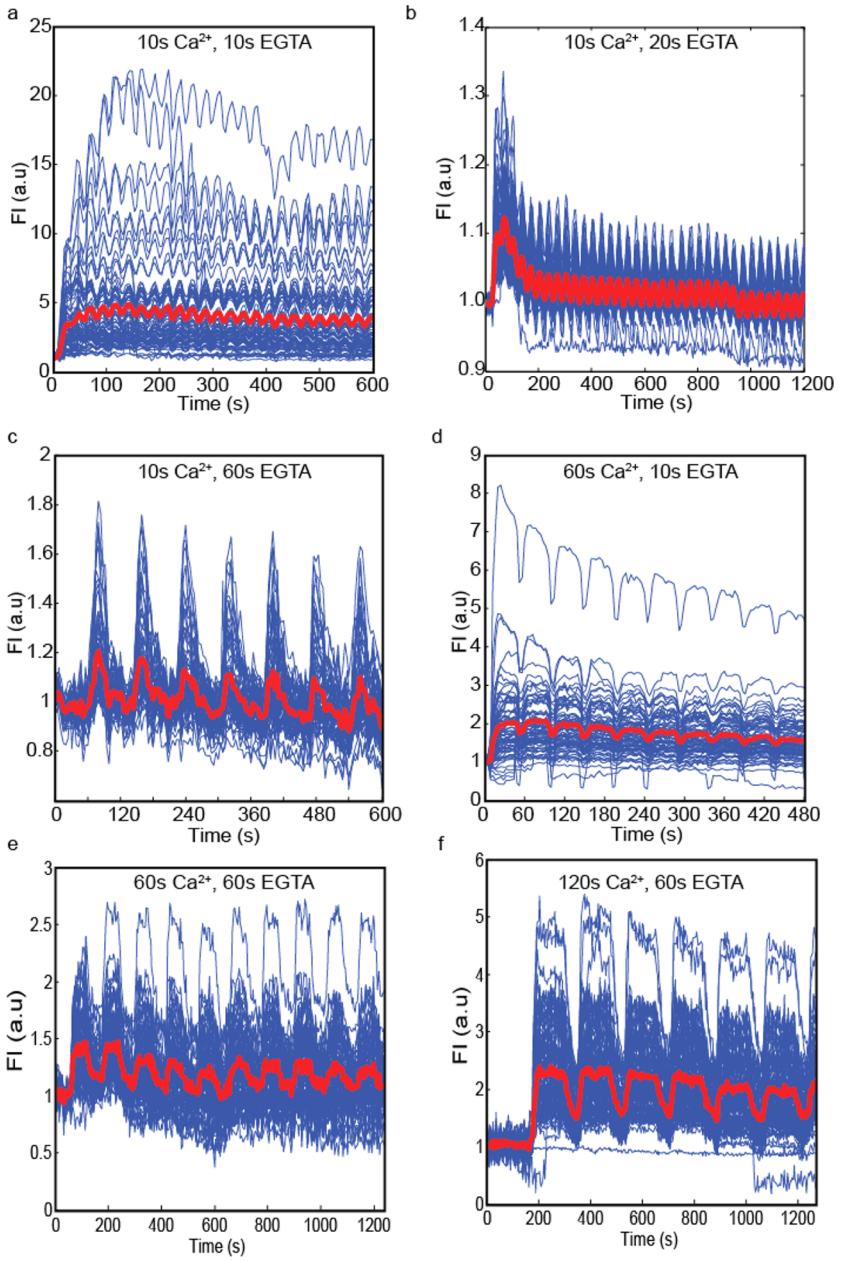

Figure 7. Individual calcium response curves at varying stimulation periodicity of hundreds of cells: (a–f) show the cytoplasmic response of individual cells (blue traces) and the average (red trace) at different stimulation durations.

the calcium response stimulation. By taking an average of the cells, the cell populations were shown to exhibit an oscillatory calcium response that was entrained with the input signal (Figure 5c). In contrast, analyzing the individual calcium response behaviors, we observed that the cells exhibited heterogeneity that can be categorized into four distinctive behavior categories (Figure 5d): oscillatory (85%), peak then plateau (7%), peak then drop to basal level (4%), and no response (4%). These distinct responses demonstrate the diverse cellular response that would be otherwise masked in cell population data, as indicated in Figure 5c, where a population average gives an oscillatory Ca^{2+} response.

To test the dynamic Ca^{2+} oscillations in Jurkat cells over a range of periodicities, we exposed the cells to Ca^{2+} pulses at varying periods. In general, the cells are entrained to the external Ca^{2+} stimuli when the frequency of the signal is not too high (Figure 6). Overall, the cells showed Ca^{2+} oscillations with diminishing amplitude over time (Figure 6a–d) in response to Ca^{2+} pulses. These calcium temporal dynamics (frequency, amplitude, and duration of oscillation) can influence which intracellular pathways are activated.[27] By modulating the temporal signal in terms of concentration, pattern, and duration of exposure, we can study how cells respond to temporally varying environments. This platform, in combination with live cell imaging and computational modeling, may be useful in elucidating signal transduction pathways present on multiple time scales. For example, dynamic input signals are an important tool in studying system dynamics both *in vitro* and *in silico* when the system in largely unknown, and systems have been studied and well characterized under oscillatory input using the frequency response analysis.[28]

dx.doi.org/10.1021/ac5019843 | *Anal. Chem.* 2014, 86, 10138–10147

To further demonstrate the utility of the device, we show individual cell response and average responses to temporal calcium. In Figure 7, individual calcium response curves (blue traces) and the average calcium response (red trace) for ∼100−150 cells are shown for stimulation at varying periodicities. The range of stimulation periodicities ranges from short periods of 10 s (Figure 7a−c) to longer periods of 2 min (Figure 7f). Overall, we have shown a device for handling a large array of cells and delivering repeatable temporal stimulation in a spatially independent manner.

CONCLUSIONS

We have developed a generalizable platform for stimulating a dense array of cells with spatially independent, temporally diverse chemical signals, while simultaneously performing fluorescence time-lapse microscopy for real-time analysis of cell response at single-cell resolution. The cell-trapping array enables us to observe hundreds of nonadherent cells simultaneously in the field of view, while the chemical delivery module allows all the cells to be exposed to the same stimulus at the same time. With this device, we have demonstrated the acquisition of the quantitative oscillatory cytoplasmic Ca^{2+} behavior of Jurkat cells exposed to Ca^{2+} pulses, which can be exploited in future experiments to study gene expression patterns in cells exposed to varying frequencies of Ca^{2+}. In addition, the stimulus delivery approach is independent of the nature of the stimulus used and only depends on the perforated membrane that can be easily modulated to suit different applications and chip designs. Our approach is generally applicable to any chip design as it involved adding functional modules to existing chip designs. The ability to deliver spatially uniform, temporally synchronized, and dynamic signal patterns over a large cell array allows us to study a large population of cells at a single cell level, rendering information on the heterogeneity of subsets within the population.

ASSOCIATED CONTENT

Supporting Information

A figure depicting the 3-dimensional rendering of the device showing the layers that make up the multilayer devices and the positioning of the cells, a cross-sectional view showing device dimensions and lumped resistance analysis, a figure showing calcium response represented as a heatmap with each trace representing individual cell response, and a figure showing the characterization of the 5 s period signal. This material is available free of charge via the Internet at http://pubs.acs.org.

AUTHOR INFORMATION

Corresponding Author

*E-mail: hang.lu@gatech.edu.

Author Contributions

The manuscript was written through contributions of all authors. All authors have given approval to the final version of the manuscript.

Notes

The authors declare no competing financial interest.

ACKNOWLEDGMENTS

We acknowledge the financial support of NIH R01 AI088023 and NSF CBET 0954578. H.L. is supported by a DuPont Young Professor Award, Alfred P. Sloan Foundation Fellowship. M.Z. is supported by an NSF Graduate Research Fellowship. C.Z. is supported by NIH R01 AI077343 and R01 AI044902. The authors acknowledge the Chemical Engineering Machine Research Services for help with machining of equipment parts used in the experiments, Emily Jackson and Ariel Kniss for feedback on the manuscript, and Ivan Caceres for help with the MATLAB image acquisition code.

REFERENCES

(1) Mettetal, J. T.; Muzzey, D.; Gómez-Uribe, C.; van Oudenaarden, A. *Science* **2008**, *319*, 482−484.
(2) Jovic, A.; Wade, S. M.; Miyawaki, A.; Neubig, R. R.; Linderman, J. J.; Takayama, S. *Mol. BioSyst.* **2011**, *7*, 2238−2244.
(3) Hersen, P.; McClean, M. N.; Mahadevan, L.; Ramanathan, S. *Proc. Natl. Acad. Sci. U.S.A.* **2008**, *105*, 7165−7170.
(4) Kim, Y.; Joshi, S. D.; Messner, W. C.; LeDuc, P. R.; Davidson, L. A. *Plos One* **2011**, *6*, No. e14624.
(5) Tomida, T.; Oda, S.; Takekawa, M.; Iino, Y.; Saito, H. *Sci. Signaling* **2012**, *5*, ra76.
(6) Velve-Casquillas, G.; Le Berre, M.; Piel, M.; Tran, P. T. *Nano Today* **2010**, *5*, 28−47.
(7) Sun, J.; Wang, J.; Chen, P.; Feng, X.; Du, W.; Liu, B. F. *Anal. Bioanal. Chem.* **2011**, *400*, 2973−2981.
(8) Kawada, J.; Kimura, H.; Akutsu, H.; Sakai, Y.; Fujii, T. *Lab Chip* **2012**, *12*, 4508−4515.
(9) VanDersarl, J. J.; Xu, A. M.; Melosh, N. A. *Lab Chip* **2011**, *11*, 3057−3063.
(10) Ahmed, D.; Chan, C. Y.; Lin, S.-C. S.; Muddana, H. S.; Nama, N.; Benkovic, S. J.; Jun Huang, T. *Lab Chip* **2013**, *13*, 328−331.
(11) Chung, K.; Zhan, M.; Srinivasan, J.; Sternberg, P. W.; Gong, E.; Schroeder, F. C.; Lu, H. *Lab Chip* **2011**, *11*, 3689−3697.
(12) Wang, C. J.; Bergmann, A.; Lin, B.; Kim, K.; Levchenko, A. *Sci. Signaling* **2012**, *5*, ra17.
(13) Awwad, Y.; Geng, T.; Baldwin, A. S.; Lu, C. *Anal. Chem.* **2012**, *84*, 1224−1228.
(14) Sochol, R. D.; Dueck, M. E.; Li, S.; Lee, L. P.; Lin, L. *Lab Chip* **2012**, *12*, 5051−5056.
(15) Chung, K.; Rivet, C. A.; Kemp, M. L.; Lu, H. *Anal. Chem.* **2011**, *83*, 7044−7052.
(16) Rettig, J. R.; Folch, A. *Anal. Chem.* **2005**, *77*, 5628−5634.
(17) Zhang, H.; Liu, K.-K. *J. R. Soc., Interface* **2008**, *5*, 671−690.
(18) Ding, X.; Lin, S.-C. S.; Kiraly, B.; Yue, H.; Li, S.; Chiang, I.-K.; Shi, J.; Benkovic, S. J.; Huang, T. J. *Proc. Natl. Acad. Sci. U. S. A.* **2012**, *109*, 11105−11109.
(19) Whitesides, G. M.; Ostuni, E.; Takayama, S.; Jiang, X.; Ingber, D. E. *Annu. Rev. Biomed. Eng.* **2001**, *3*, 335−373.
(20) Thastrup, O.; Cullen, P. J.; Drøbak, B. K.; Hanley, M. R.; Dawson, A. P. *Proc. Natl. Acad. Sci. U. S. A.* **1990**, *87*, 2466−2470.
(21) Edelstein, A.; Amodaj, N.; Hoover, K.; Vale, R.; Stuurman, N. *Computer Control of Microscopes Using μManager*; John Wiley & Sons, Inc.: New York, 2010.
(22) Garanich, J. S.; Mathura, R. A.; Shi, Z. D.; Tarbell, J. M. *Am. J. Physiol.: Heart Circ. Physiol.* **2007**, *292*, H3128−H3135.
(23) Dalous, J.; Burghardt, E.; Muller-Taubenberger, A.; Bruckert, F.; Gerisch, G.; Bretschneider, T. *Biophys. J.* **2008**, *94*, 1063−1074.
(24) Liu, B. Y.; Chen, W.; Evavold, B. D.; Zhu, C. *Cell* **2014**, *157*, 357−368.
(25) Arrol, H. P.; Church, L. D.; Bacon, P. A.; Young, S. P. *Clin. Exp. Immunol.* **2008**, *153*, 86−95.
(26) Dolmetsch, R. E.; Xu, K.; Lewis, R. S. *Nature* **1998**, *392*, 933−936.
(27) Dolmetsch, R. E.; Lewis, R. S.; Goodnow, C. C.; Healy, J. I. *Nature* **1997**, *386*, 855−858.
(28) Geva-Zatorsky, N.; Dekel, E.; Batchelor, E.; Lahav, G.; Alon, U. *Proc. Natl. Acad. Sci. U. S. A.* **2010**, *107*, 13550−13555.